We are IntechOpen,
the world's leading publisher of
Open Access books
Built by scientists, for scientists

6,900
Open access books available

186,000
International authors and editors

200M
Downloads

Our authors are among the

154
Countries delivered to

TOP 1%
most cited scientists

12.2%
Contributors from top 500 universities

CLARIVATE ANALYTICS

BOOK CITATION INDEX

INDEXED

WEB OF SCIENCE™

Selection of our books indexed in the Book Citation Index
in Web of Science™ Core Collection (BKCI)

Interested in publishing with us?
Contact book.department@intechopen.com

Numbers displayed above are based on latest data collected.
For more information visit www.intechopen.com

Chapter 10

Series Elastic Actuator: Design, Analysis and Comparison

Arnaldo Gomes Leal Junior,
Rafhael Milanezi de Andrade and
Antônio Bento Filho

Additional information is available at the end of the chapter

Abstract

In general, actuators are built to be as stiff as possible to increase the bandwidth. When a robot works in a structured environment, its automation is easier than in a non-structured environment in which case its modeling is quite difficult and presents a high computational effort. To overcome this difficulty, series elastic actuator (SEA) has been applied in compliant robotic grasping. Unlike rigid actuators, a SEA contains an elastic element in series with the mechanical energy source. Such an elastic element gives SEAs tolerance to impact loads, low mechanical output impedance, passive mechanical energy storage, and increased peak power output. The spring has to be able to support the loads, but it cannot be too stiff; otherwise, system impedance will be high. This chapter describes a comparison between two types of SEA, an electric series elastic actuator (ESEA) and a hydraulic series elastic actuator (HSEA), for four-legged dynamic robot application. The parameters employed in the comparison are bandwidth, output impedance, time response, power density, and dynamic range. The results indicate that HSEA is a better actuator than ESEA for a weight carrying four-legged dynamic robot because of its higher power density and dynamic ratio with desirable output impedance, time response, and bandwidth.

Keywords: SEA, actuator, force control, dynamic robot, legged robot

1. Introduction

1.1. Force control

Over the years, the premise for constructing machines and actuators is "Stiffer is better" since a stiffer actuator has larger bandwidth force control and accurate position control. On the other

hand, the force control is difficult since it develops high forces from small displacement and a little position error can result in a large force error. For this reason, the sensor has to be very precise with good resolution. Moreover, a stiffer actuator can lead to accidents with humans in a non-structured environment.

The majority of standard robot actuation systems cannot create precise force on the robotic joints due to friction, stick-slip, backlash and reflected inertia through the transmission, cogging in motors, and pressure drop in hydraulic circuits, among others. However, even with these nonlinearities and noises on force measurements, some robots are well aligned for a position or trajectory control since the mass of the robot and actuators acts as a low-pass filter for the force on position output (Robinson, 2000).

In some tasks, such as precise load positioning and human joints actuation, a good force control is required. In this case, the force noise on the actuators will hinder the application of the standard robot actuation. To achieve a good force-controlled system, some parameters have to be measured which are force bandwidth, mechanical output impedance, dynamic range and force density. All these parameters are related with each other and are further discussed in Section 4.

Although standard robots and stiff actuators are not good in force control, the humans are. Moreover, humans have no problems in contact hard surfaces and perform precise operations. Based on this bioinspiration, Williamson (1995) began to sacrifice the bandwidth and the stiffness for more stable force control. The method applied is to place an elastic element in series with the power source which are, commonly, a DC motor with gear reduction or a hydraulic cylinder (**Figure 1**).

Figure 1. Series elastic actuator schematic (Williamson, 1995).

1.2. Series elastic actuators

Series elastic actuator (SEA) has been successfully applied in a number of applications for almost 20 years (Pratt and Williamson, 1995). As widely reported by a number of researchers (see Pratt and Williamson, 1995; Arumugom et al., 2009; Paluska and Herr, 2006; Paine et al., 2013), SEA provides many benefits in force control of robots. Series elastic actuators have an elastic element attached with the mechanical energy source output. This configuration presents advantages over rigid actuators such as low mechanical output impedance, tolerance to impact loads, increased peak power output, and passive mechanical energy storage. These properties enable the application of SEAs in legged actuation systems and human orthotics (Pestana et al., 2010; Parietti et al., 2011).
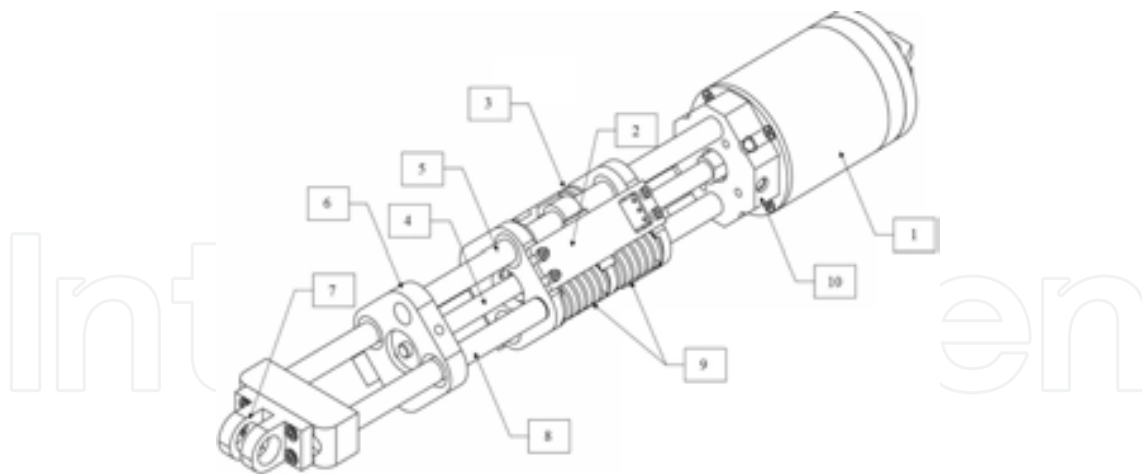
Figure 2. Electric SEA (1) DC motor with gearbox; (2) moving sub assembly, (3) ball nut plate, (4) ball screw, (5) guide rod, (6) support plate, (7) load connection terminal, (8) moving rod, (9) and springs (10) motor angle and rods plate (Pratt et al., 2002).

Figure 2 shows a linear electric driven SEA (Pratt et al., 2002). The DC motor with gearbox (1) drives the ball screw (4) which moves the ball nut plate (3). Ball nut plate (3) then moves the springs (9) against the moving sub-assembly (2) which is fixed to the moving rods (8), thus causing the displacement of the load connection terminal (7) and then moves the load. The guide rods (5) are fixed to the motor flange (10) and to the support plate (6) through plain bearings for the ball screw and for the moving rods (8). They move together with the moving sub-assembly (2) in which they are fixed. It follows that all the force exerted by the spindle motor assembly on the load is directly supported by the springs, which are the elastic element purposely inserted to lower the stiffness of the actuator load interface.

The SEA's designs are made under various trade-offs, and the decision parameters often are power output, volumetric size, weight, efficiency, Back-drivability, impact resistance, passive energy storage, backlash, and torque ripple. Furthermore, iterations may be necessary on components design of a SEA. Curran and Orin (2008), Hutter et al. (2009), Kong et al. (2009), and Ragonesi et al. (2011) propose rotary designs based primarily on commercially available off-the-shelf components. Lagoda et al. (2010) and Diftler et al. (2011) design a compact rotary SEA using a harmonic drive and a high-stiffness planar spring. A compact actuator can be achieved by placing linear springs coupled to rotary shafts between the motor and the chassis ground as presented in Hutter et al. (2011) and Torres-Jara and Banks (2004). Furthermore, this compact actuator employs springs with low stiffness. In order to reduce the torque requirement on the spring, Kong et al. (2012) and Taylor (2011) placed the spring within the reduction phase. A promising design for SEA that is widely researched throughout the years is to apply ball screws as the primary reduction mechanism followed by a cable drive which remotely drives a revolute joint. This design takes advantage of the ball screw high efficiency even for large speed reductions (85–90%), backdrivability, impact tolerance, and do not introduce torque ripple (Edsinger-Gonzales and Weber, 2004; Gregorio et al., 1997; Pratt and Pratt, 1998). Paine et al. (2013) presented a good review of some recent progress in series elastic actuators. In this chapter, we presented a different design of SEA. In order to avoid accidents

risks and components contamination, the internal components were encapsulated in a unique hollow tubular structure. This allows the substitute of the heavy structure of solid steel tubes of the reference model (Pratt et al., 2002), permitting the applications in wearable robots, exoskeletons and prostheses.

Regarding the control of series elastic actuators, as can be expected, the design of the controller is closely related to the hardware employed. Therefore, a controller parameter such as the output force can be estimated by measuring spring deflection (Kong et al., 2010), or by applying strain gauges (Pratt and Williamson, 1995). Nevertheless, a PID approach for force control suffers from stability issues if friction and backlash are too large. For this reason, an impedance control is developed, which basically is an innermost control structure with position feedback to treat the force control as a simple position or velocity control (Pratt et al., 2004; Lagoda et al., 2010). In this chapter, such idea was adopted to develop the proposed SEA controller.

1.3. Series elastic actuator background

The first robot designed with SEA was the Spring Flamingo (Pratt and Pratt, 1998) which is a planar bipedal walking robot. The SEAs drive six degrees of freedom mechanism which has three degree of freedom in each leg representing hip, knee and ankle. **Figure 3** shows the Spring Flamingo, it can walk at 1.25m/s on flat terrain. Moreover, it can walk over uphill and downhill terrains up to 15 degrees slope.

Figure 3. Spring Flamingo (Pratt and Pratt, 1998).

The extension of the work started with the Spring Flamingo is the M2 (Robinson et al., 1999) which is a three-dimensional bipedal walking robot. For this reason, it has twelve degrees of freedom, six on each leg. Regarding one leg, the M2 has three degrees of freedom on the hip, two degrees of freedom on the ankle, and one degree of freedom on the knee. This configura‐ tion provides three-dimensional movements with the same characteristics of the Spring

Flamingo. The M2 project is far more complex than the Spring Flamingo, as can be seen in **Figure 4**.
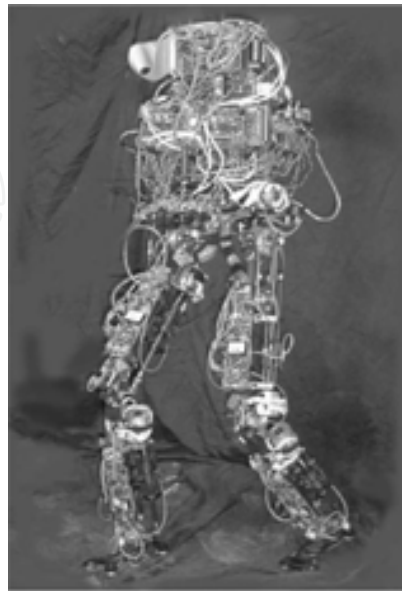

Figure 4. M2 (Robinson et al., 1999).

Another lower limb robot developed with SEA is the Corndog (Krupp, 2000) which is a planar running robot with one fore and one aft leg. Therefore, it represents only the half of a dog and employs electro-mechanical series elastic actuator (**Figure 5**).
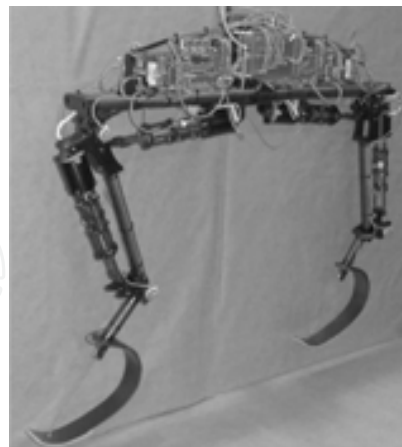

Figure 5. The Corndog (Krupp, 2000).

Series elastic technology is also applied on upper limb robots. The COG robot is a humanoid with upper torso and head (Brooks et al., 1999). It has 6 degrees of freedom on its arms which are operated with SEAs. Moreover, COG has the ability to hammering and turning a crank (**Figure 6**).
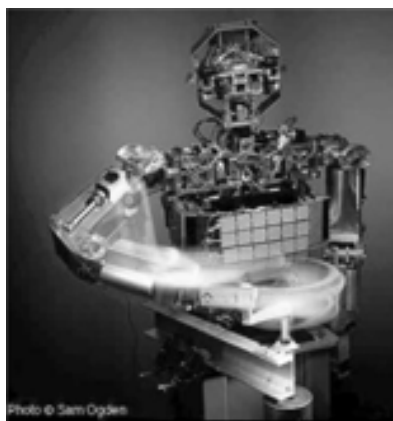
Figure 6. COG humanoid robot (Brooks et al., 1999).

In addition to the application on dynamic robots, SEAs have been widely studied and applied on rehabilitation and assistive technologies. Regarding assistive technologies for gait rehabilitation, a compact rotary SEA for knee joint assistive exoskeleton is developed (Kong et al., 2010). Unlike the majority of SEAs with motor and gear reduction as the motor part, a worm gear is used for motor reduction due to it compactness. However, it increases the friction of the system, which makes it more difficult to control (**Figure 7**). A robust control algorithm inspired by disturbance observer is implemented for the system control.
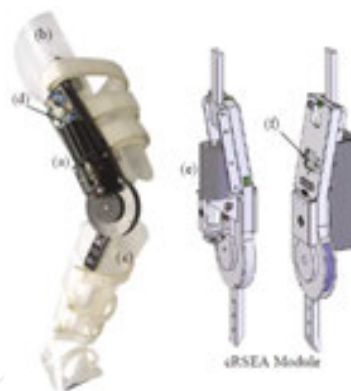

Figure 7. Proposed exoskeleton for knee assistance. (a) Rotary SEA module, (b) a thigh brace, (c) a calf brace, (d) a motor driver, (e) a DC motor, and (f) an controller (Kong et al., 2010).

Lagoda et al. (2010) designed a Series elastic actuated joint for robotic gait rehabilitation training to be applied at LOPES (Lower Extremity Powered Exoskeleton) which helps an impaired patient to training his/her gait with an assisted-as-need (AAN) approach which only provides actuated torque as needed to help the patient to complete the gait cycle.

Series elastic actuator is also employed on assistive technologies, a prosthetic knee is developed and the stiffness adjustments are described to achieve the optimum values for peak power and energy consumption for walking and running (Grimmer and Seyfarth, 2011). Results have shown large reductions in peak power and energy requirements with the proper spring

selection. Moreover, SEA can mimic the human knee behavior better than the passive approaches.

Au et al. (2007) proposed a prosthetic ankle comprised of SEA that matches size and weight of the human ankle, comparing with the passive approaches, SEA ankle prosthesis enhances the capability of mimicking the human gait (**Figure 8**).

Figure 8. Ankle-foot prosthesis (Au et al., 2007).

Another approach for human-friendly actuators for assistive robotic application is to add a variable damping in the SEA design as shown in **Figure 9**. It can be achieved with magneto-rheological fluids (MR fluids).
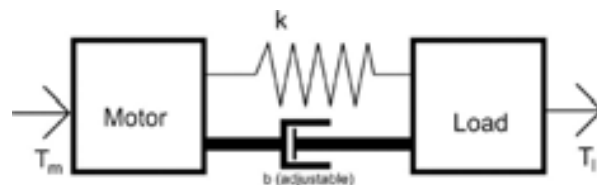

Figure 9. Series elastic actuator with controlled damping (Iyer, 2012).

Although this configuration allows a human-friendly device that can be applied to design legs with agile locomotion (Garcia et al., 2011), the investigation of such devices are beyond this chapter analysis, but will be investigated in further works.

2. Electric series elastic actuator

2.1. Electric series elastic actuator design

Over the years, digital prototyping has been successfully applied in engineering and manufacturing allowing virtually explore a complete product before it's built (Thurfjell et al., 2002;

Soyguder and Alli, 2007; Wang, 2011). As reported by Johansson et al. (2004), the digital prototyping has been important to the development of industrial robots, reducing the time of robot programming phase. According to the authors, the robot task can be simulated in a virtual model of the workcell when still only a digital prototype of the workpiece exists and the risk of technical failure for a transition can be reduced. In this way, before manufacture of the proposed serial elastic actuator, its digital prototyping is presented in this chapter.

2.1.1. First design

The characteristics desired for the actuator are enclosed internal components, to avoid component contamination and accidents risks; size adequate for wearable robots, exoskeletons and prostheses applications, emulating natural muscles; aesthetically suited to applications in wearable robots, exoskeletons and prostheses; and smart enough for applications in unstructured environment.

Figure 10. First prototype showing internal actuator components: ball screw (1); ball nuts (2); movable arm (3); springs (4, 5); motor & gearbox (6); base tube (7); bearing screw (8); O-ring (9); Allen screws (10); guide ring (11).

The first prototype design is shown in **Figure 10**. There are two ball nuts (2) bolted to plates with a tab and grooved flanges for O-rings (9) installation. The flanges have a central hole and are connected by means of an extender, which is a tube with external male thread at both ends. The springs (4 and 5) slide around the extender and press on both sides a plate fixed to the tube base (7) of the retractable arm (3).

2.1.2. The moving sub-assembly

Figure 11 shows the exploded view of the moving sub assembly, a set of pieces that behaved as a single device after assembled. Two bolted flanges (4, 3) enclose the ball nut (1). Tubes (2) are used to grip a flange on the nut (1). The flange (4) has threaded holes for Allen screws (5) and flange (3), countersunk holes for these screws and thread. In the central bore of each flange is a threaded guide tube (6), with the pre stressed springs. The circuit board (7) is fixed over the flanges with the sensor for acquiring the deformation of the spring against the linear encoder attached to the flanges (3) and (4).
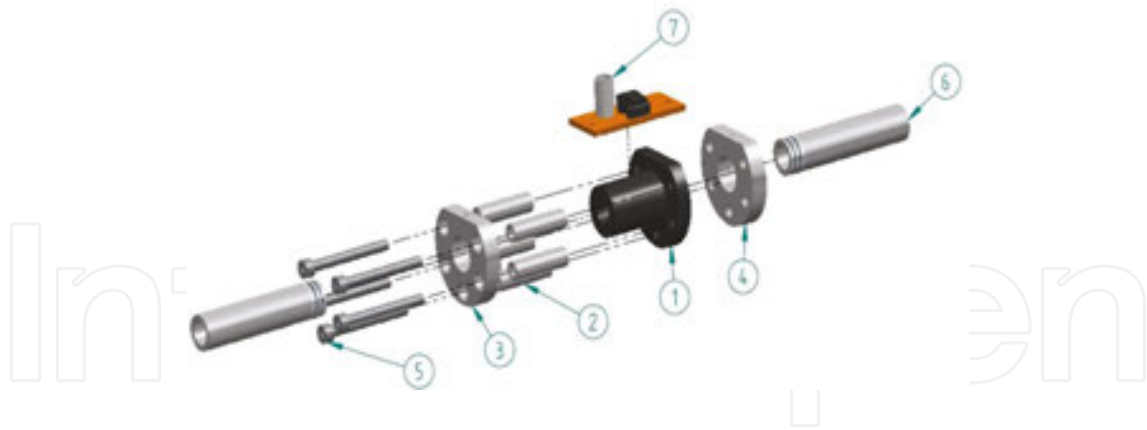
Figure 11. Exploded view of the final design action sub assembly components.

2.1.3. DC motor and gearbox

It was chosen based on the forces for actuator operation and for the spring assembly, according to the planetary gearbox, and the ball screw torque force conversion. The DC motor is a 60 mm, brushless, 400 W; the gearbox is a planetary gearhead 62 mm diameter, 8–50 N.m torque and the ball screw is a 10 mm diameter and 3 mm pitch rolled steel.

2.1.4. Final design

Figure 12 shows the actuator final design. The iterative digital prototyping design process done resulted in a set of desirable characteristics for the actuator very similar to those originally intended, which are 425 mm long when retracted, with 130 mm range with maximum diameter of 60 mm. For the sake of wider range of operation, the model has interchangeability of springs. The ball screw has 10 mm diameter and 3 mm pitch. Main model structure of carbon steel and aluminum alloy tubes allows a final weight of 3.7 kg. The operating voltage of the ESEA is 48 V. These model's properties allows a 450 N maximum load capacity and 13.4 cm/s continuous speed.

Figure 12. Actuator final design with internal components.

2.2. Dynamic model

The dynamic model of the actuator was constructed from the digital prototype data to run a simulation in order to verify its dynamic behavior, bandwidth and validate the project settings, as presented in **Figure 13**.
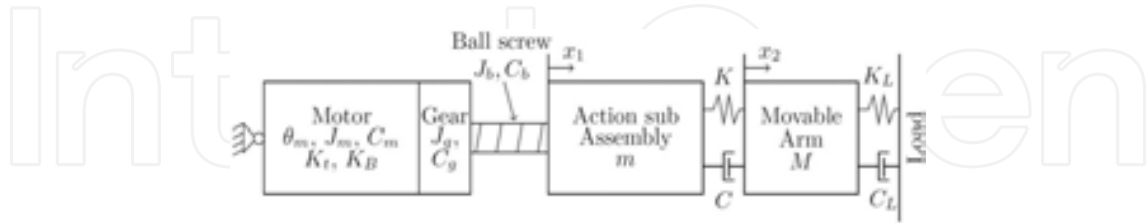

Figure 13. Actuator's mechanical model.

Referring to **Figure 13**, the actuator dynamic model equations are described as follows:

$$L_a \frac{di_a}{dt} + R_a i_a + K_b \omega = V_a \tag{1}$$

In Eq. (1), L_a is the armature inductance, i_a is the armature current, R_a is the armature resistance, K_b is the back Electromotive Force (back-EMF) constant, ω is the angular velocity, and V_a is the armature voltage.

$$J_T \ddot{\theta}_m + C_T \dot{\theta}_m = k_t i_a \tag{2}$$

Referring to Eq. (2), J_T is the total inertia of the actuator, C_T is the total viscous friction coefficient, θ_m is the angular displacement velocity of the motor axis, $\ddot{\theta}$ is the motor angular acceleration, and k_t is the motor torque proportional constant.

The SEA's total inertia referred in Eq. (2) is the summation of all inertia effects presented by each component as depicted in Eq. (3).

$$J_T = \left[J_m + J_g + n^2 J_b + \left(\frac{np}{2\pi} \right)^2 m \right] \tag{3}$$

where J_m is the rotor inertia, J_g is the gear inertia, n is the gear ratio, J_b is the ball screw inertia, p is the ball screw pitch, m is the action device sub assembly mass.

A similar approach is applied to evaluate the total viscous friction coefficient presented in Eq. (2). The summation of all the friction effects results in the total viscous friction coefficient (Eq. (4))

$$C_T = \left[C_m + C_g + n^2 C_b + C \left(\frac{np}{2\pi} \right)^2 \right] \tag{4}$$

Referring to Eq. (4), C_m is the rotor viscous friction coefficient, C_g is the gear reduction viscous friction coefficient, C_b is the ball screw viscous friction coefficient, C is the action sub assembly viscous friction coefficient.

In Eqs. (5) and (6), Newton's second law is applied on the movable arm and action sub assembly systems to evaluate the action sub assembly and movable arm displacement in order to estimate the spring deflection.

$$m\ddot{x}_1 + C_b x_1 = m \left(\frac{np}{2\pi} \right) \ddot{\theta}_m + C_b \left(\frac{np}{2\pi} \right) \dot{\theta}_m = f \tag{5}$$

$$M\ddot{x}_2 + C_L x_2 + K_L x_2 = f \tag{6}$$

where f is the force between action sub assembly and the movable arm, M is the movable arm sub assembly mass, C_L is the load interface viscous friction coefficient, and K_L is the load interface elastic constant. The term $\left(\frac{np}{2\pi} \right)$ is the linear displacement of the movable arm reflected to motor axis rotation, and $\left(\frac{np}{2\pi} \right)^2$ is the inertia and viscous friction components of the action device reflected to motor axis.

Once the actuator dynamic model equations are described, the closed loop PID transfer function block diagram in the frequency domain can be made, as shown in **Figure 14**.
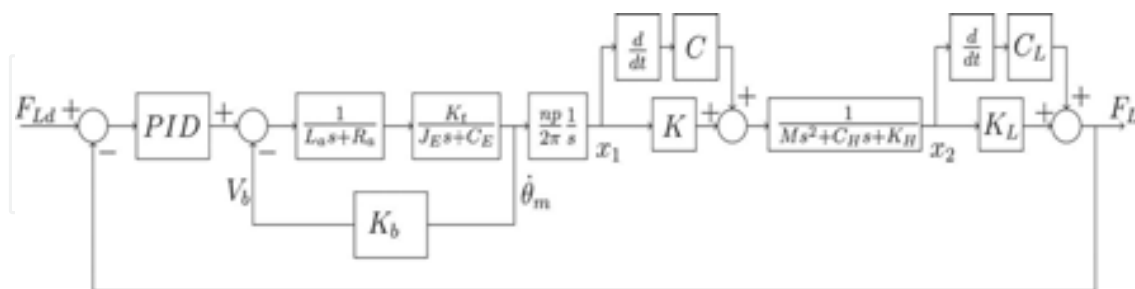

Figure 14. Actuator's closed loop transfer function block diagram.

2.3. Results and discussion

Once the actuator dynamic model has been described, the parameter values had to be established. The parameters were obtained by the digital prototype design and data sheets of some components, i.e. motor and ball screw (**Table 1**).

Spring constant is the most important parameter in the system. To define the spring constant, we set the minimum impedance level and a maximum bandwidth with respect to the previous selected components of the system. Iteration was made to choose the best value with upper and lower bounds.

After knowing all the actuator's parameters, the PID controller could be designed. The controller was tuned by applying the pole placement and phase margin method (Tang et al., 2010). The same PID control tuning strategy is applied in the controller of the linear serial elastic hydraulic actuator (Leal Junior et al., 2015). For this reason, applying the same tuning method in the electric SEA helps on further responses comparison between the hydraulic and the electric SEA.

Parameter	Value	Units
Armature inductance (La)	8.2E–04	(H)
Armature resistance (Ra)	1.03	(Ω)
Total inertia (JT)	9.51E–05	(kg m^2)
Mass (M)	1.261	(kg)
Total viscous friction (CT)	4.594E–05	(Ns/m)
Arm and load stiffness (KH)	3.336E+06	(N/m)
back-EMF constant (Kb)	1.469E–01	(Vs/rad)
Load stiffness (KL)	3.303 +06	(N/m)
Load damping (CL)	8.08	(Ns/m)
Spring stiffness (K)	3.27E+04	(N/m)
Spring viscous friction (C)	8.000E–01	(Ns/m)
Torque proportional constant (KT)	1.470E–01	(Nm/A)
Gear ratio (n)	0.001	(1)
Ball screw pitch (p)	0.003	(m)

Table 1. Parameters value of the entire ESEA system.

Desired pair of poles is estimated by representing time domain specification, e.g. percent overshoot, settling time. However, in some cases the dominant poles lose its dominant position in the result of the closed loop system. To overcome this problem, a phase margin is employed to guarantee the closed loop system robustness.

Assuming a pair of poles as

$$p_{1,2} = -\alpha \pm j\beta \qquad (7)$$

The process G(s) is given and the controller has its conventional configuration with all positive gains as follows.

$$C(s) = K_p + \frac{K_i}{s} + K_d s \tag{8}$$

Substituting one of the poles into the characteristic equation of the closed loop equation which is the transfer function denominator of the process G(s).

$$1 + G(p_1)C(p_1) = 0 \tag{9}$$

Moreover, the definition of phase margin gives:

$$G(j\omega_g)C(j\omega_g) = -e^{j\varphi_m} \tag{10}$$

Substituting and splitting the complex values and the real ones of Eqs. (9) and (10) gives two real functions of (Eqs. (11) and (12)).

$$f_1(\omega) = \mathrm{Re}\left[\frac{-p_1}{G(p_1)}\right] + \frac{\alpha^2 - \beta^2}{2\alpha\beta}\mathrm{Im}\left[\frac{-p_1}{G(p_1)}\right] + \frac{\alpha^2 + \beta^2}{2\alpha}\mathrm{Re}\left[\frac{-e^{j\varphi_m}}{G(j\omega)}\right] \tag{11}$$

$$f_2(\omega) = \frac{\omega^2}{2\alpha}\mathrm{Re}\left[\frac{-e^{j\varphi_m}}{G(j\omega)}\right] - \frac{\omega^2}{2\alpha\beta}\mathrm{Im}\left[\frac{-p_1}{G(p_1)}\right] - \omega\,\mathrm{Im}\left[\frac{-e^{j\varphi_m}}{G(j\omega)}\right] \tag{12}$$

The positive values of the intersection between $f_1(\omega)$ and $f_2(\omega)$ are the first approximation for integral gain (K_i). This first value was applied on Eqs. (13) and (14) to evaluate the proportional and derivative gains. Proportional and derivative gains are obtained by substituting the well-known PID controller equation C(s), presented in Eq. (8), in Eqs. (9) and (10).

$$K_p = \frac{2\alpha}{\alpha^2 + \beta^2}\left(K_i - \mathrm{Re}\left[\frac{-p_1}{G(p_1)}\right] - \frac{\alpha^2 - \beta^2}{2\alpha\beta}\mathrm{Im}\left[\frac{-p_1}{G(p_1)}\right]\right) \tag{13}$$

$$K_d = \frac{1}{\alpha^2 + \beta^2}\left(K_i - \mathrm{Re}\left[\frac{-p_1}{G(p_1)}\right] - \frac{\alpha}{\beta}\mathrm{Im}\left[\frac{-p_1}{G(p_1)}\right]\right) \tag{14}$$

The final integral gain is the maximum value between Eqs. (15) and (16).

$$K_{i,1} = \left(\text{Re}\left[\frac{-p_1}{G(p_1)} \right] - \frac{\alpha}{\beta} \text{Im}\left[\frac{-p_1}{G(p_1)} \right] \right) \tag{15}$$

$$K_{i,2} = \left(\text{Re}\left[\frac{-p_1}{G(p_1)} \right] - \frac{\alpha^2 - \beta^2}{2\alpha\beta} \text{Im}\left[\frac{-p_1}{G(p_1)} \right] \right) \tag{16}$$

To achieve a robust control with large bandwidth it was set an overshoot about 10% and a settling time of 0.02 s. Phase margin was set 60°. **Table 2** shows the integral, proportional and derivative gains of the ESEA's controller.

Parameter	Value
Proportional gain (Kp)	2.915
Integral gain (Ki)	4.129
Derivative gain (Kd)	0.007

Table 2. Controller parameters.

Figure 15 shows the Bode diagram of the system, there is a good frequency band of 40 Hz, compatible with the Paine's results (Paine et al., 2013). On the other hand, the phase angle is quite high at 40 Hz, greater than 90°. Yet it is possible to apply the actuator in several systems where force control is necessary, as in some robot arms in industrial plants. Resonance frequency is greater than 200 Hz. This implies that the effects due to vibrations are efficiently filtered into the frequency band of the actuator.
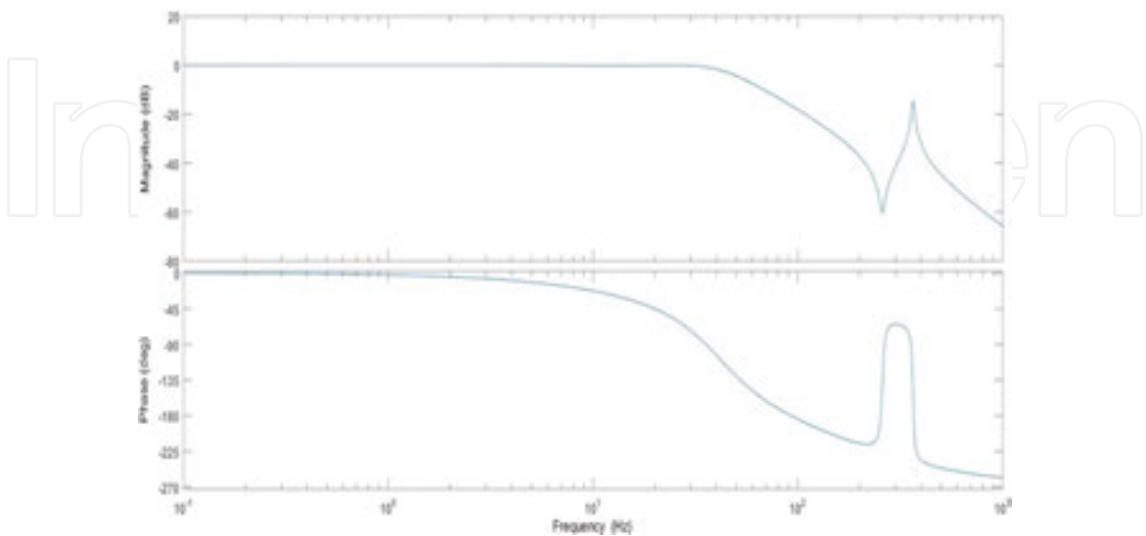

Figure 15. Bode diagram of the system.

Figure 16 shows the time response for a constant input force. The electric SEA shows an 8% overshoot and it settling time is 0.03 s which is very fast. While hydraulic SEA of reference work (Leal Junior et al., 2015) has an overshoot about 12% and a settling time of 0.07 s. Although hydraulic SEA has larger overshoot and settling time than electric SEA of this section, these two parameters are compatible with the reference works results (Paine et al., 2013; Robinson, 2000). Therefore, even in the Hydraulic SEA case the settling time is tolerated which is discussed in Section 4.

2.4. Final remarks

This section presented the digital prototyping of a linear electric SEA for exoskeletons, wearable robots and mechatronic devices. It was used as a digital prototyping environment for design and assembly of actuators parts, generation of section views images in perspective and exploded views, and all fabrication drawings of the actuator parts. The prototype is driven by a Maxon EC 60 Ø60 mm, brushless 400W DC motor, with a Planetary Gearhead GP 62 A (Maxon Motor Catalogue) and an R Series 10mm diameter rolled steel ball screw (NSK Catalogue).

This section also presented the actuator's performance, evaluated under a PID impedance controller. **Figure 15** shows the frequency response of the magnitude and phase of Fl/Fd. **Figure 16** shows the step response of unit force input. The step response can also be tuned to final displacement or to contact force. Some improvements to the actuator itself will be needed for the next steps of the project, aiming at the fabrication, assembly and testing of the actuator.

Future works are the construction of a real aluminum alloy based prototype and testing its performance in a real time environment to evaluate the actuator's performance under force,
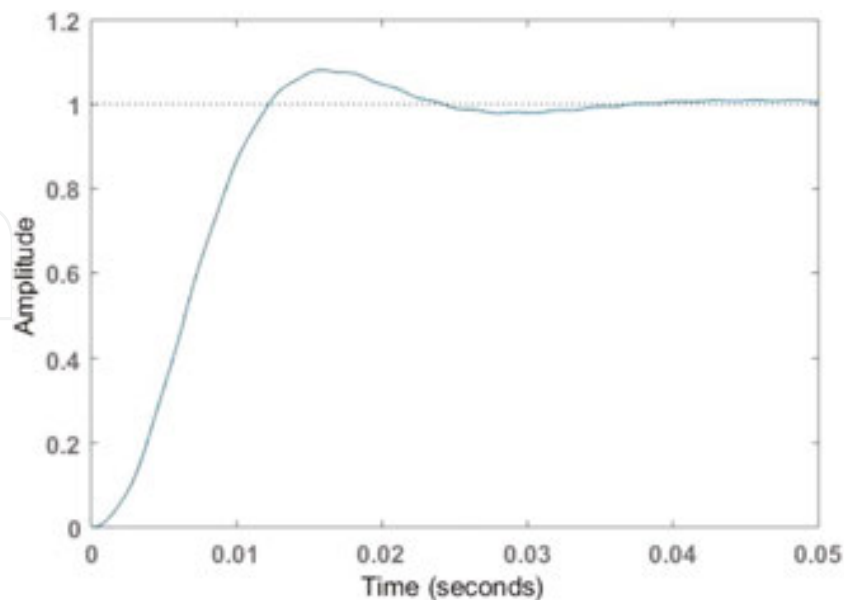

Figure 16. Time response for a 1N step input force.

position, velocity and mixed controllers. It is also important to verify the effect of spring stiffness and gear ratio in load bandwidth. Another further investigation is the development of tuning strategies between the spring stiffness – actuator bandwidth and elastic energy store relationship. Since these effects were neglected in this section, actuator's backslash and viscous friction have to be analyzed in future works.

A broad comparison between the electric serial elastic actuator and the hydraulic SEA has to be made to define which one is the best for a compliant robot application.

3. Hydraulic series elastic actuator

3.1. Hydraulic series elastic actuator design

3.1.1. Methodology

A basic model of a series elastic hydraulic actuator has the serial element, i.e. a rod with the spring's arrangement and a hydraulic circuit which basically comprises of the hydraulic cylinder and the servo valve. The actuator may be understood as a combination of two parts. The first one is the serial elastic element presented. The other one is the hydraulic circuit which has some construction alternatives as well.

Once the hydraulic circuit and serial elastic element of the actuator are defined, the next step is to select the hydraulic components and design the spring based on the application. This is done by defining a condition for this system which, in this case, is the actuator output force to be up to 5000 N. To achieve this output force, the springs are selected based on consolidate knowledge presented by mechanical engineering design bibliography. Moreover, the rod had to be able to support the load without buckling. A special attention must be given to the actuator's springs because they affect system's impedance and bandwidth. After setting these two parameters, iteration could be necessary to evaluate the desirable spring constant.

After the selection of the rod and the spring, it is possible to use the force caused by the spring under allowable extension-compression limits as the force output of the hydraulic cylinder. This force and the maximum speed of 0.5 m/s, as defined by Robinson and Pratt (2000), led to the selection of the correct cylinder by a commercial data sheet; otherwise it would be possible to manufacture a custom cylinder. After the parts design, they are assembled in Siemens Solid Edge (Siemens PLM Software, Germany) digital prototyping environment which allows obtaining inertial properties of the assembly.

3.1.2. Digital prototyping design

The design was done by the methodology mentioned on the previous section. Following these steps, the actuator achieved a good volume-output force ratio for the available components combination. Also all the internal components had been enclosed to avoid accidents, components contamination and make the actuator suitable to human interaction (Bento Filho et al., 2014).

Figure 17 shows the prototype of the actuator. There is a hydraulic cylinder (1) that moves forward and dislocates the movable rod (2) fixed in it with a screwed connection. The model has two low friction sliding cylinders (6) and (8) fixed on the base tube (3) and one guide (7) fixed on the movable rod (2). There are two springs (4) and (5) fixed between the low friction sliding cylinders (6) and (8). A connection guide (10) is used to connect the hydraulic cylinder rod (1) to the base tube (3). The load terminal (9) is also connected directly on the base tube (3). The encapsulation tube (12) is the last part of the assembly. It is connected on the hydraulic cylinder (1) and base tube (3). A guide bolt (11) was applied to make the connection between the base tube (3) and the encapsulation tube (12), but without interfere on the base tube's (3) linear movement.

Figure 17. Actuator's components: (1) hydraulic cylinder; (2) movable rod; (3) base tube; (4) and (5) springs; (6), (7) and (8) low friction sliding cylinders; (9) load terminal; (10) connection guide; (11) guide bolt; (12) encapsulation tube.

There are four low friction sliding cylinders (6), (7), (8), and (10) in this actuator model. The application of the four sliding cylinders is to give to the system the necessary stability. Without these components, the movable rod (2) would oscillate creating additional forces on the springs instead of only an axial force. Moreover, the load terminal is connected with the base tube only.

The springs are responsible to the hydraulic SEA stiffness reduction. However, this component has to be carefully assembled since it will stretch and compress depending on the movement of the actuator and the load attached to it. Choosing the spring is always challenging, because it has to be a balance between a large bandwidth requiring a high stiffness and impedance that needs a low spring constant. Therefore, after choosing all system characteristics and components, a minimum acceptable point must be defined between the largest force bandwidth and the minimum tolerance impedance level. After setting these two bounds, iteration is required to estimate the spring constant.

The movement of the actuator can be analyzed in three different cases:

Case 1: Movement without load

This is the simplest case, because it is a free movement. The hydraulic cylinder moves forward or backward and the movable rod and all the others components attached to it such as base tube, guides and load terminal follow the movement of the hydraulic cylinder. In this case, there is only a little deflection in the springs due to system's inertia.

Case 2: Movement with load

When a load is attached in the load terminal, the movement of the actuator depends on the springs. For a forward movement, the spring (5) deflects and spring (4) stretches due to springs preload. These deflections and stretching depends on the load mass. The actuator moves forward only when the spring's deformation resulting force equals the applied load. This system characteristic can reduce the frequency range and makes a limit of bandwidth of the system, which is the major drawback of a series elastic actuator.

For the backward movement the same characteristics can be observed, but the spring (4) deflects and spring (5) stretches.

Case 3: Contact of the load terminal with the load

When the actuator reaches an obstacle or the load during its free movement, the springs deform and the value of the resulting force makes the actuator continues its forward movement or stop.

The prototype shows outstanding characteristics of output force and compactness. The actuator has 200 mm length when retracted with 100 mm of range. The maximum diameter is 26 mm. Moreover, with 100 bar of working pressure, this SEA produces output force up to 4.9 kN which is a great power to weight ratio since the estimated weight of the actuator is 1.5 kg. In order to ease the manufacturing, model structure material chosen is the carbon steel. Actuator's parameters are measured for modeling and control purposes. Important parameters are the deflection of the springs and the displacement of the movable rod, which are due the movement of the hydraulic cylinder.

A linear potentiometer was chosen to evaluate the movable rod's displacement. Since the potentiometer did not have the resolution to evaluate the deflection of the springs, an optical sensor used on a printer was chosen to evaluate this deflection. This sensor has a scaled tape with black lines, with distance between the lines known, which does not allow light beam passage. The tape movement produces pulses, which are proportional to spring deflection.

The assembly of the sensors was shown in **Figure 18**. The linear potentiometer (3) was connected directly on the hydraulic cylinder rod (2) and the hydraulic cylinder bore (1). The optical sensor has a circuit board (7) with a sensor (9). This circuit board was connected on the sliding cylinder (6) by a bolt connection. The optical tape (8) was connected on the sliding cylinders (4) and (5) by a bolt connection and positioned on the optical sensor (9).
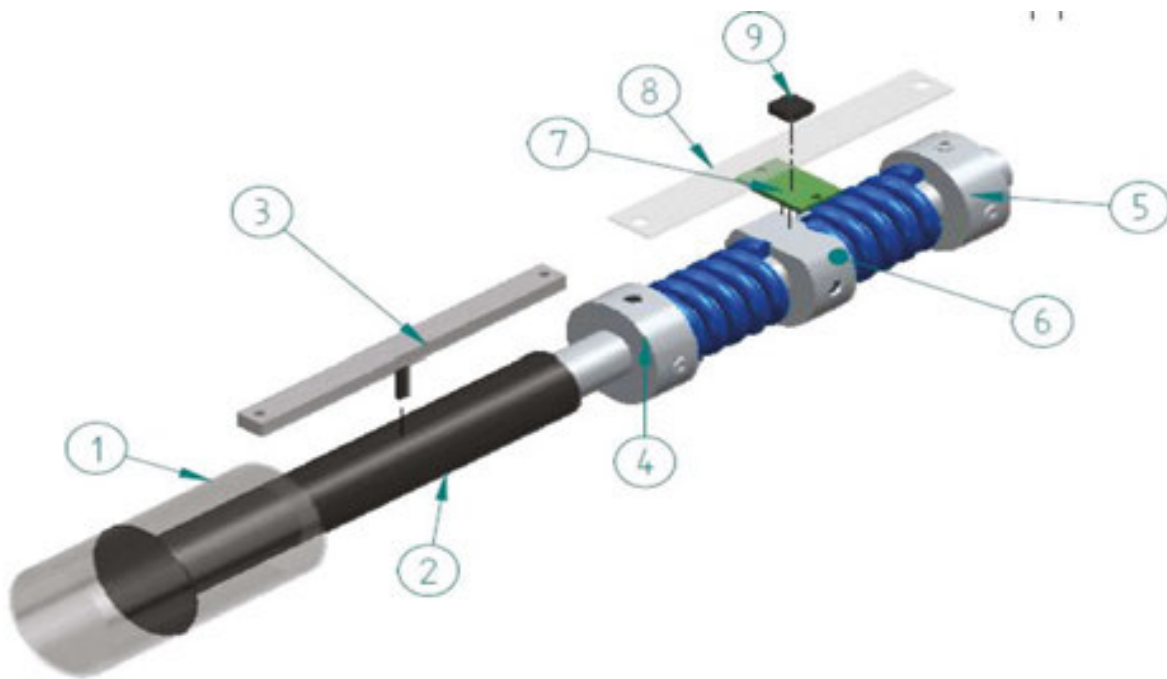
Figure 18. Sensors assembly: (1) hydraulic cylinder bore; (2) hydraulic cylinder rod; (3) linear potentiometer; (4), (5) and (6) guides; (7) circuit board; (8) optical sensor tape; (9) optical sensor.

3.2. Dynamic model

The system consists of a servo-hydraulic system with a serial elastic element. The overall system has two degrees of freedom. One degree is the hydraulic cylinder displacement and the other is the serial elastic element displacement. This displacement and the spring deflection were used to define the output force of the system and to control it. **Figure 19** illustrates the mechanical model of this system discussed above.
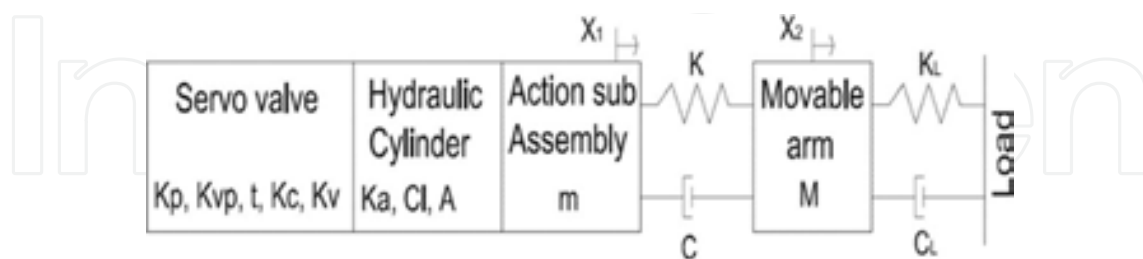

Figure 19. Actuator's mechanical model.

Although most of the servo-hydraulic system is nonlinear, each component of this model has been linearized (Qian et al., 2014). The linearization occurs at an operating point and also can be made at multiple operating points. The controller is tuned based on the linearized model. Although an actuator does not work at a fixed operation point, the controller based on a linearized system has good response even when it is off the operation point.

The servo valve's pilot stage is assumed to be of first order. Since high order dynamics in the valve are more than an order of magnitude above the frequency range of 40 Hz which is the frequency of interest (Robinson and Pratt, 2000), the higher order dynamics can be neglected. Eq. (17) represents the servo valve pilot stage equation as seen in Qian et al. (2014).

$$\frac{Q_s(s)}{v_i(s)} = \frac{K_{vp}}{\tau s + 1} \times K_p \times K_C \times K_v \tag{17}$$

where K_{vp} is the flow gain of the pilot-stage servo valve and τ pilot-stage's equivalent time constant, v_i valve control signal transmitted from the hydraulic system internal proportional controller, K_p represents inner loop proportional gain, K_C is the valve pressure gain which relates flow from the pilot stage with spool position. The coefficient K_v is the flow gain of the servo valve and Q_s is the supply flow. Rearranging the flow terms and applying the well-known cylinder force equation gives Eq. (18) (Qian et al., 2014).

$$\frac{F_A(s)}{Q_s(s)} = \frac{\dfrac{4}{\beta V s + C_l} \times A}{1 + \dfrac{4}{\beta V s + C_l} \times A^2 \times X_1(s) s} \tag{18}$$

This β is the fluid bulk modulus, V is the fluid volume, A is the cross sectional area, $X_1(s)$ is the action sub-assembly displacement.

The serial elastic element has to be modeled by Newton's second law (Eq. (19)). The properties of the movable rod and the springs are considered on the stiffness, damping and mass terms. The load characteristics are also considered in the actuator's dynamic model (Eq. (20)).

$$X_1(s)(ms^2 + Cs + K) = F(s) \tag{19}$$

where $X_1(s)$ is the action sub-assembly displacement, m is the action sub-assembly mass, C is the damping coefficient, K is the stiffness coefficient and F is the output force.

$$X_2(s)(Ms^2 + C_L s + K_L) = F(s) \tag{20}$$

Referring to Eq. (20), M is the movable arm mass, C_L and K_L are the load interface viscous friction coefficient and load interface elastic constant respectively. $X_2(s)$ is the movable arm displacement. The simplified closed loop transfer function block diagram for the dynamic model is presented in **Figure 20**. Each subsystem presented in the figure has a transfer function according the equation discussed on this topic. The actuator was modeled to have a natural velocity feedback (Qian et al., 2014). The leakage of the servo valve stages was neglected. The

assumptions made in this model are constant fluid properties, servo valves are not saturated, supply pressure is much greater than the load pressure, friction force can be modeled as viscous damping, main stage spool opening is proportional to pilot stage flow (Qian et al., 2014) **Figure 20** shows the hydraulic SEA block diagram.
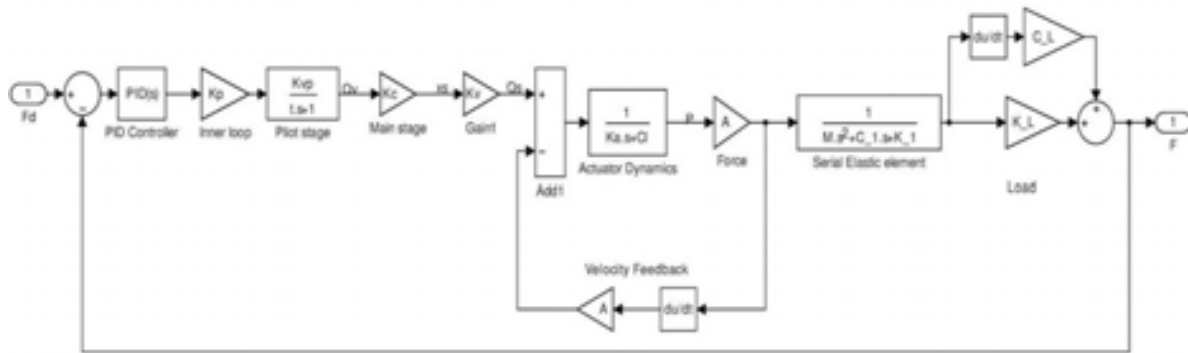

Figure 20. Closed loop transfer function block diagram.

3.3. Results and discussion

Once the actuator dynamic model is described, the parameter values had to be established. The parameters were obtained by the digital prototype and data sheets of some components i.e. servo valve and hydraulic actuator. **Table 3** summarizes the HSEA parameters applied on dynamic model.

Parameter	Value	Units
Area (A)	4.91E–04	(m^2)
Stiffness (K1)	7.5E+07	(N/m)
Damping (C1)	18.4	(Ns/m)
Mass (M)	1.5	(Kg)
Bulk modulus (B)	1.23E+09	(Pa)
Leakage coefficient (Cl)	2E–06	(m^{3}s/kPa)
Fluid volume (Vt)	2.60E–05	m^3
Load stiffness (KL)	3.30E+09	(N/m)
Load damping (CL)	8.08	(Ns/m)
Inner loop gain (Kp)	8.40E+02	(s^{-1})
Valve pressure gain (Kc)	4.00E+06	(m^{3}s/m)
Valve flow gain (Kv)	6.24E–05	(m^{3}s/m)
Servo valve time constant (t)	0.0015	(s)

Table 3. HSEA parameters.

Spring constant is the most important parameter in the system. To define the spring constant, the minimum impedance level and a maximum bandwidth were set with respect to the previously selected components of the hydraulic system. Iteration was made to choose the best value with upper and lower bounds.

After knowing all the actuator's parameters, the PID controller could be designed. The controller was tuned by applying the pole placement and phase margin method presented in Section 2. A PID controller is able to produce good responses. This controller is widely applied on industrial robots and processes due to its robustness and simple implementation.

To achieve a robust control with large bandwidth, an overshoot of about 10% and a settling time of 0.02 s were set. Phase margin was set to 60°. **Table 4** shows the controller parameters for the system's characteristics aforementioned.

Parameter	Value
Proportional gain (Kp)	54.9946
Integral gain (Ki)	4412.1219
Derivative gain (Kd)	0.0575

Table 4. Controller parameters.

The bode diagram of the system (**Figure 21**) shows an excellent frequency band of about 100 Hz which was greater than all references works presented (Bento Filho et al., 2014; Paine et al., 2013; Robinson and Pratt, 2000). The phase angle for this frequency band was around 45°. The resonance frequency of the system was 1100 Hz which is far enough to the system's operation frequency. This implies that the effects due to vibrations are efficiently filtered into the frequency band of the actuator.
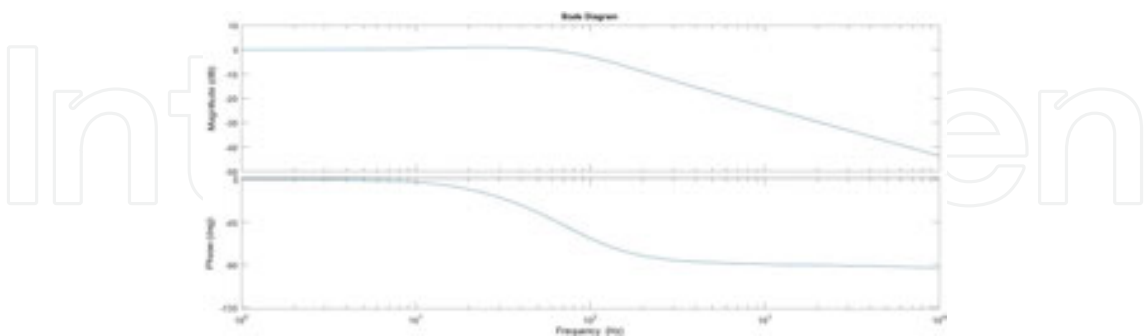

Figure 21. Bode diagram of the system.

To show the system's response, a Unit step input was applied. **Figure 22** shows the system's response where it could be seen that the settling time is around 0.02 s which was a very fast convergence to this system. The maximum overshoot was a little higher than 10% which was an acceptable value.
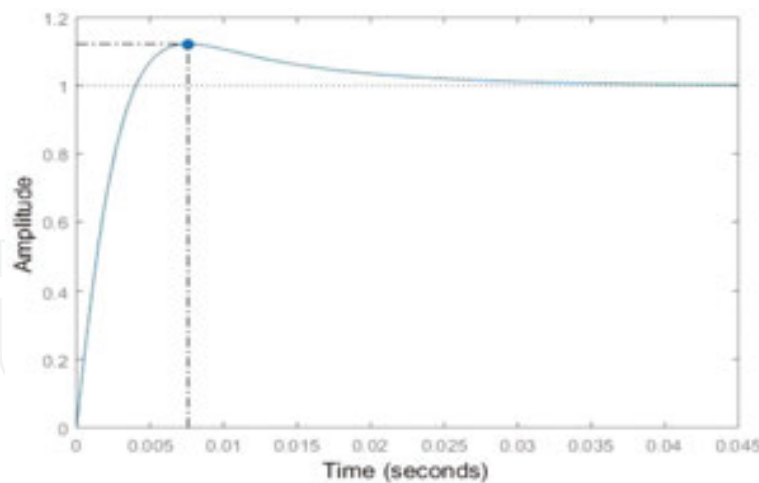
Figure 22. Time response of the system.

3.4. Final remarks

This section presented a digital prototyping of a linear series elastic hydraulic actuator for compliant robots. It was used in digital prototyping environment for design and assembly of actuators parts, generation of images of section views in perspective and exploded views, and all fabrication drawings of the parts of the actuator. The model obtained was very compact with a high output force which is desirable for all applications. A dynamic model with a PID controller was also presented which described the linear characteristics of the actuator. The system showed good time and frequency responses. The results obtained help the development of robots and manipulators for non-structured environments with another level of compactness and force capacity.

Future work is the construction of the actuator and investigation of benefits and limitations of this actuator on a compliant robot with human interaction.

4. Comparison between series elastic actuators

4.1. Comparison parameters

As mentioned in Section 1, the analysis of an actuator comprises the investigation of force bandwidth, mechanical output impedance, dynamic range, force density and the time response for the system without load. Each of these parameters has its own importance for the system and its own method to be determined. Robinson (2000) first introduced the comparison methodology adopted in this chapter. In these analyses, the load stiffness and viscous damping presented for ESEA and HSEA presented in **Tables 1** and **3** respectively is not considered on the following analyses. Therefore, it is expected that the systems responses have deviations between the ones presented in Sections 2 and 3.

4.1.1. Force bandwidth

The force bandwidth of an actuator is how quickly it can generate the desired forces. In order to be able to perform the desired task, the bandwidth must be sufficiently high to transmit the forces through the machine structure. To control a human joint, only a few Hertz of bandwidth is necessary. Moreover, the bandwidth needed for a four-legged dynamic robot for weight carrying is small too. Reference authors estimate that only 20 Hz is more than necessary for the given application. The bandwidth analysis is divided in the closed loop force bandwidth and the large force bandwidth. Closed loop bandwidth is evaluated with a step input of a small force in the actuator closed loop model (**Figure 23**). The large force bandwidth is obtained with an oscillation of the full steady-state output force of the actuator as an input on the closed loop model. HSEA has 4.9 kN of output force and ESEA has only 450 N. Due to this difference between the actuators capabilities, only the closed loop bandwidth is compared in this chapter. Referring to **Figure 23**, X_m is the motor displacement, F_d is the desired force, F_l is the output force, k_s is the spring stiffness, K and V_c are model characteristics.
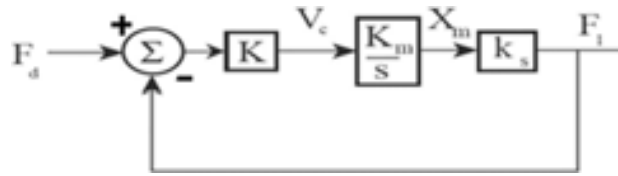

Figure 23. Simplified block diagram for closed loop bandwidth evaluation (Robinson, 2000).

4.1.2. Mechanical output impedance

The mechanical output impedance is defined as the minimum force needed to move a certain load. An actuator with low impedance can be considered a pure force source since its internal dynamics are negligible. Low impedance actuators can also be referred as back-drivable (Robinson, 2000). The analysis of the output impedance is made by applying to each actuator model the case of a load, which is free to move, attached to the actuator's output. The impedance is evaluated around a constant desired output force as an analogy of the concept of impedance on electrical circuits (**Figure 24**). Referring to **Figure 24**, the x_l is the load displacement, x_s is the spring displacement and F_l is the force output.
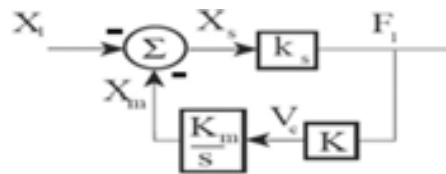

Figure 24. Simplified block diagram for mechanical output impedance evaluation (Robinson, 2000).

4.1.3. Dynamic range

The dynamic range is the ratio between the maximum output force of the actuator and the minimum resolvable force of this device. The dynamic range analysis on an actuator is very important since it gives a measure of how sensitive the actuator is to small force compared to the actuator maximum force. For example, if an actuator has high maximum force and high minimum resolvable force, its dynamic range is low. Therefore, this actuator can only make tasks of high force and it is not able to manipulate fragile objects or have direct contact with humans. Moreover, a large dynamic range is desirable for almost all robotic applications, since it allows the robot to be versatile to perform high sensitive operations and large force demanding operations. Since it can sense or grasp almost all fragile objects and manipulate it in precise tasks and, on the same time, can perform high force demanding tasks such as weight lift, one of the largest dynamic range actuator is the human muscle.

4.1.4. Force density

Force density is defined as the ratio between the output force and the mass or the volume of an actuator. An actuator with large force density allows the application in lighter robots with good force output characteristics since it not overburden the robot structure and allows the quick response of the mechanism.

4.2. Results and discussion

The two SEA presented in previous sections are compared based on the key parameters of the series elastic actuators aforementioned which are bandwidth, output impedance, time response, power density, dynamic range.

The spring stiffness affects all parameters presented above. In order to evaluate the differences between the two systems with the same parameter for the compliant sensor, the spring stiffness is 3.336E+03 kN/m for both actuators.

4.2.1. Force bandwidth results

Figure 25 shows the HSEA and ESEA Bode diagram which allows evaluating the two systems closed loop force bandwidth.
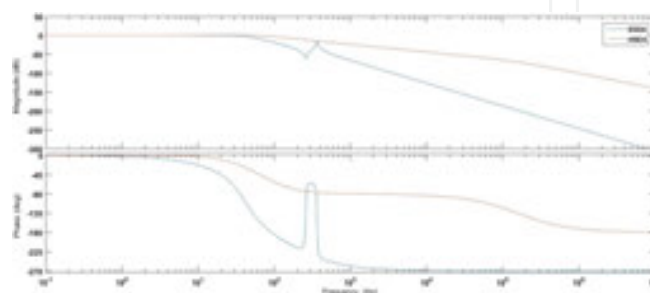

Figure 25. Closed loop bode diagram.

The ESEA frequency band is about 40Hz with a phase angle of 90° which is quite high. On the other hand, the HSEA has 30Hz but the phase angle is about 55° which is more appropriate for practical applications. Since a four-legged robot works on small bandwidths, the smaller bandwidth range of the HSEA is not an issue for this application. In addition, the two actuators present resonance frequency above 100Hz which is far enough to the required frequency.

4.2.2. Time response results

The time response for a Unit step input of the system without the load is given in **Figure 26**. In the ESEA and HSEA design made in Sections 2 and 3, respectively, the system dynamic has a load damping of 8 Ns/m and a load stiffness of 3E+06 N/m. ESEA shows an 8% overshoot and settling time of 0.03 s which is very fast. While HSEA has an overshoot about 12% and a settling time of 0.07 s. Although HSEA has larger overshoot and settling time than ESEA, these two parameters are compatible with the reference works results (Paine et al., 2013; Robinson, 2000). Therefore, even in the HSEA case the settling time is tolerated.
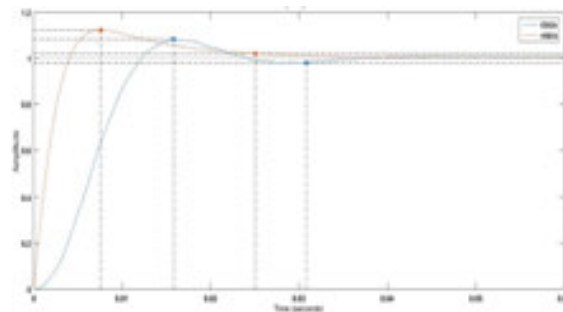

Figure 26. Time response of the actuators.

4.2.3. Mechanical output impedance results

Since output impedance is the force at an actuator output given a moving load position, the impedance analysis was made by setting a load position with a constant desired force. An ideal actuator has zero impedance. In other words, the actuator is a pure force source. If this happens, the dynamics of the actuator are completely decoupled from the dynamics of the load motion (Robinson, 2000). Although the compliant element of the series elastic actuator limits the bandwidth, it reduces the output impedance which is desirable for many actuator applications (Pratt et al., 2002).

Nevertheless, these two actuation systems have the same spring stiffness. Therefore, the differences between the systems output impedance are due to the actuator's moving system which are the motor with gear reduction for the ESEA and servo valve with hydraulic piston for the HSEA (Robinson, 2000).

Figure 27 shows the output impedance for both hydraulic and electric sources. The output impedance of the series elastic actuator is small at low frequency and it achieves the spring stiffness magnitude (which is −130dB for the spring previous selected) when the frequency

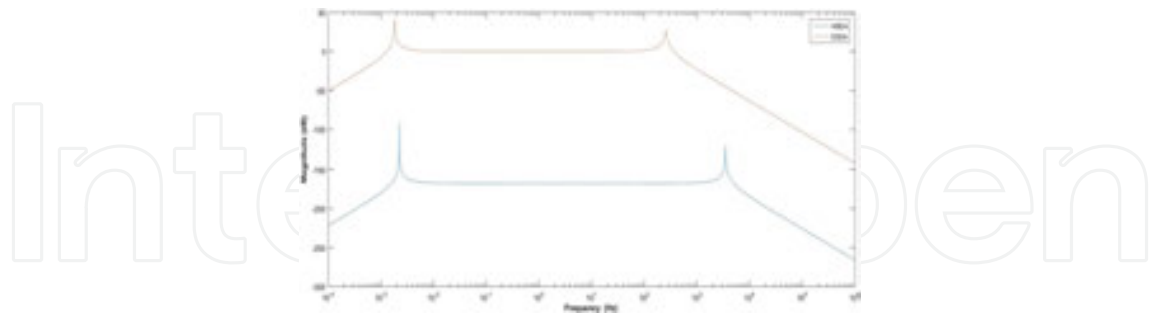rises. This behavior was proved by simulations and physical SEA experiments (Robinson, 2000).

Figure 27. HSEA and ESEA output impedance.

Since the both systems have the same compliant element, they achieve the same value with frequency increase. Therefore, the difference on the impedance is given by the curve slope. Examining the slope of the both curves, the HSEA has the smallest value of the impedance when the frequency increases. It can be seen two peaks of the magnitude, the first one due to controller gains and the second occurs in the systems resonance frequency.

4.2.4. Power density results

Power density is the actuator power per mass unit. High power density actuators can delivery great power with a small package. It prevents over-burdening the actuator structure with excessive mass allowing a responsive robot performance. The lightweight structure with a quick performance is very important for a weight carrying dynamic robot because it provides a compact robot which is suited to a non-structured environment and has a great output force.

As shown in previous section, the hydraulic series elastic actuator has more output force than the electric SEA. Moreover, the ESEA is heavier than the HSEA.

The output force of the HSEA is 4.9kN and it weighs 1.5kg given the velocity of 0.5m/s, the HSEA has a power density about 1600W/kg which is a great performance. On the other hand, the ESEA has 450N of output force and weighs 3.7kg. The ESEA is also slower than HSEA, the electric SEA velocity is 13.4cm/s which gives a power density of 16W/kg. This result shows a poor performance of ESEA for weight carrying dynamic robot.

Even though the HSEA mass applied on the power density calculation did not include the mass of servo valve, reservoir, pump, hoses and pipes which are heavier than the ESEA batteries that also are not included on the electric SEA mass. Even if these accessories mass is considered, the HSEA still has way more power density even with these items included.

4.2.5. Dynamic range results

Dynamic range is the ratio between the maximum output force and the minimum resolvable output force. It gives quantitative information of how sensitive the actuator is with respect of

its maximum output force capability. It is a crucial parameter for dynamic robots because it allows the actuator to be used in sensitive activities such as human contact, equipment operation, and non-structured environment exploration. In addition, the actuator with great dynamic range can do hard work activities such carrying, push or pull weights. In summary, high dynamic range is an important characteristic for a four-legged dynamic robot application.

The minimum resolvable output force is evaluated by the resolution of the spring deflection sensor. Resolution gives the minimum spring deflection that can be detected. This deflection times the spring stiffness gives the actuator minimum resolvable force.

Both the SEAs have the same spring stiffness in this comparison. Also, both actuators have the same spring deflection sensor which is a linear encoder. Therefore the minimum output force is the same for both which is 3N.

The HSEA dynamic range is 1500:1 while the ESEA range is 150:1. It shows that the hydraulic SEA has a range 10 times bigger than electric one.

5. Conclusions

This chapter presented a comparison between the two series elastic actuator (electric SEA and hydraulic SEA) for four-legged dynamic application. The actuators were digitally prototyped and the comparison was made considering actuator's bandwidth, output impedance, time response, power density, and dynamic range.

Although the ESEA has a better time response, both actuators have its responses within desired range for a dynamic robot application. The bandwidth also is not a problem for both actuators because all systems examined have large bandwidth compared with the given application. HSEA and ESEA presented good output impedance with a slightly better behavior from hydraulic SEA. Both actuators have two peaks on the output impedance, one peak due to controller gains and another due to the resonance frequency of the system.

Power density and dynamic range are the two key parameters that differs the weight carrying dynamic robot application from others dynamic robots applications. In these two parameters, the HSEA showed a better performance than ESEA. The HSEA's power density is 100 times higher than the ESEA's. Moreover, the dynamic range of hydraulic SEA is 10 times higher than the electric SEA dynamic range. The results showed the HSEA as the better series elastic actuator for this task and it could contribute for the research of SEA applied on robot links.

Further work is required on the simulation of SEA, specially the HSEA, on a dynamic robot. With this simulation, the advantages and drawbacks of the implementation can be analyzed and quantified. Also, a construction of a real aluminum alloy based prototype and testing its performance in a real time environment for evaluating the actuator's performance under force, position, velocity and mixed controllers. Another future work is on the development of tuning strategies between the spring stiffness – actuator bandwidth and elastic energy store relationship.

Author details

Arnaldo Gomes Leal Junior[1], Rafhael Milanezi de Andrade[1,2*] and Antônio Bento Filho[1]

*Address all correspondence to: rafhael.andrade@ufes.br

1 Department of Mechanical Engineering, Universidade Federal do Espirito Santo, Vitória, ES, Brazil

2 Department of Mechanical Engineering, Bioengineering Laboratory, Universidade Federal de Minas Gerais, Belo Horizonte, MG, Brazil

References

[1] Arumugom, S., Muthuraman, S., and Ponselvan, V., "Modeling and application of series elastic actuators for force control multi legged robots," J. Comput., vol. 1, no. 1, pp. 26–33, 2009.

[2] Au, S., Weber, J., Herr, H., "Biomechanical design of a powered ankle-foot prosthesis" in IEEE 10th International Conference on Rehabilitation Robotics, 2007.

[3] Bento Filho, A., Andrade, R., Mattos, M., (2014). "Digital prototyping of a series elastic actuator for exoskeletons" in CONEM 2014.

[4] Brooks, R., Breazeal, C., Marjanovic, M., Scassellati, B., Williamson, M., "The Cog project: Building a humanoid robot" in Springer-Verlag Lecture Notes in Computer Science Volume, 1999.

[5] Curran S., and Orin, D., "Evolution of a jump in an articulated leg with series-elastic actuation," in Proc. IEEE Int. Conf. Robot. Autom., May 2008, pp. 352–358.

[6] Diftler, M., Mehling, M., Abdallah, M., Radford, N., Bridgwater, L., Sanders, A., Askew, R., Linn, D., Yamokoski, J., Permenter, F., Hargrave, B., Piatt, R, Savely, R., and Ambrose, R., "Robonaut 2—The first humanoid robot in space," in Proc. IEEE Int. Conf. Robot. Autom., May 2011, pp. 2178–2183.

[7] Edsinger-Gonzales, A., and Weber, J., "Domo: A force sensing humanoid robot for manipulation research," in Proc. IEEE/RAS 4th Int. Conf. Humanoid Robot., Nov. 2004, vol. 1, pp. 273–291.

[8] Garcia, E., Arevalo, J., Munoz, G., Gonzalez-de-Santos, P. "Combining series elastic actuation and magneto-rheological damping for the control of agile locomotion" in Robotics and Autonomous Systems vol. 59, pp. 827–839, 2011.

[9]   Gregorio, P., Ahmadi, M., and Buehler, M., "Design, control, and energetics of an electrically actuated legged robot," IEEE Trans. Syst., Man, Cybern. B, Cybern., vol. 27, no. 4, pp. 626–634, 1997.

[10] Grimmer, M., Seyfarth, A., "Stiffness Adjustment of a Series Elastic Actuator in a Knee Prosthesis for Walking and Running: The Trade-off between Energy and Peak Power Optimization" in 2011 IEEE/RSJ International Conference on Intelligent Robots and Systems, 2011.

[11] Hutter, M., Remy, C., and Siegwart, R., "Design of an articulated robotic leg with nonlinear series elastic actuation," in Proc. 12th Int. Conf. Climb. Walking Robot. Supp. Technol. Mobile Mach., Sep. 2009, pp. 645–652.

[12] Hutter, M., Remy, C., Hoepflinger, M., and Siegwart, R., "ScarlETH: Design and control of a planar running robot," in Proc. IEEE/RSJ Int. Conf. Intell. Robot. Syst., Sep. 2011, pp. 562–567.

[13] Iyer, S., "Modeling and Testing of a Series Elastic Actuator with Controllable Damping" Master's thesis, Worcester Polytechnic Institute, 2012.

[14] Johansson, R., Robertsson, A., Nilsson, K., Brogårdh, T., Cederberg, P., Olsson, M., Olsson, T., Bolmsjö, G., "Sensor integration in task-level programming and industrial robotic task execution control", Industrial Robot: An International Journal, vol. 31, no. 3, pp.284 – 296, 2004

[15] Kong, K., Bae, J., and Tomizuka, M., "A compact rotary series elastic actuator for human assistive systems," IEEE/ASME Trans. Mechatronics, vol. 17, no. 2, pp. 288–297, Apr. 2012.

[16] Kong, K., Bae, J., and Tomizuka, M., "Control of rotary series elastic actuator for ideal force-mode actuation in human-robot interaction applications," IEEE/ASME Trans. Mechatronics, vol. 14, no. 1, pp. 105–118, Feb. 2009.

[17] Kong, K., Bae. J., Tomizuka, M., "A compact rotary series elastic actuator for knee joint assistive system," in Proc. IEEE Int. Conf. Robot. Autom., May 2010, pp. 2940–2945.

[18] Krupp, B., "Design and control of a planar robot to study quadrupedal locomotion". Master's thesis, Massachusetts Institute of Technology, 2000.

[19] Lagoda, C., Schouten, A., Stienen, A., Hekman, E., and van der Kooij, H., "Design of an electric series elastic actuated joint for robotic gait rehabilitation training," in Proc. IEEE 3rd RAS and EMBS Int. Conf. Biomed. Robot. Biomechatron., Sep. 2010, pp. 21–26.

[20] Leal Junior, A., Andrade, R, Bento Filho, A.(2015). "Linear serial elastic hydraulic actuator: digital prototyping and force control", in IFAC-Papers Online, vol. 8, no. 6, pp. 279-285.

[21] Maxon Motor Catalogue, available in >www.http://www.maxonmotor.com/medias/sys_master/root/8816809443358/15-320-EN.pdf<. Accessed in 04/02/2014.

[22] NSK Catalogue, available in >http://www.nsk.com.br/upload/file/B02.pdf<. Accessed in 04/02/2014.

[23] Pestana, J., Bobin, R., Arevalo, J. C., and Garcia., E., "Characterization of emerging actuators for empowering legged robots," presented at the 13th Int. Conf. Climbing and Walking Robots Support Technologies Mobile Machines, Nagoya, Japan, 2010.

[24] Paine, N., Oh, S., and Sentis, L., "Design and control considerations for high-performance series elastic actuators" IEEE/ASME Trans. Mechatronics, vol. PP, no. 99, pp. 1–12, 2013.

[25] Paluska, D. and Herr, H., "Series elasticity and actuator power output," in Proc. IEEE Int. Conf. Robot. Autom., May 2006, pp. 1830–1833.

[26] Parietti, F., Baud-Bovy, G., Gatti, E., Riener, R., Guzzella, L., and Vallery, H.,"Series viscoelastic actuators can match human force perception," IEEE/ASME Trans. Mechatronics, vol. 16, no. 5, pp. 853–860, Oct. 2011.

[27] Pratt J., and Pratt, G., "Intuitive control of a planar bipedal walking robot," in Proc. IEEE Int. Conf. Robot. Autom.,May 1998, vol. 3, pp. 2014–2021.

[28] Pratt, G. and Williamson, M., "Series elastic actuators," in Proc. IEEE/RSJ Int. Conf. Intell. Robot. Syst. Human Robot Interact. Cooper. Robot., Aug. 1995, vol. 1, pp. 399–406.

[29] Pratt, G., Willisson, P., Bolton, C., and Hofman, A., "Late motor processing in low-impedance robots: Impedance control of series-elastic actuators," in Proc. Amer. Control Conf., Jul. 2004, vol. 4, pp. 3245–3251.

[30] Pratt, J., Krupp B., and Morse C., "Series elastic actuators for high fidelity force control", Industrial Robot: An International Journal, vol. 29, no 3, p. 234–241, 2002.

[31] Qian, Y., Ou G., Maghareh, A., Dyke, S.J.."Parametric identification of a servo-hydraulic actuator for real-time hybrid simulation," in Mechanical Systems and Signal Processing, vol. 48, pp 260–273, 2014

[32] Ragonesi, D., Agrawal, S., Sample, W., and Rahman, T., "Series elastic actuator control of a powered exoskeleton," in Proc. IEEE Annu. Int. Conf. Eng. Med. Biol. Soc., Sep. 2011, pp. 3515–3518.

[33] Robinson, D., Pratt, J., Paluska, D., Pratt, G., "Series Elastic Actuator development for a biomimetic walking robot" in IEEE/ASME AIM99, 1999.

[34] Robinson, D.,"Design and analysis of series elasticity in closed-loop actuator force control", Ph.D. Thesis, Massachusetts Institute of Technology, 2000.

[35] Siemens PLM Software – Solid Edge ST7, available in >http://www.plm.automation.siemens.com/en_us/products/solid-edge/index.shtml<. Accessed in 04/02/2014.

[36] Soyguder, S., Alli, H., "Design and prototype of a six-legged walking insect robot", Industrial Robot: An International Journal, vol. 34, no. 5, pp. 412-422, 2007

[37] Tang, W., Huang, J., Wu, J., Wang, Q., "A PID tuning method based on dominant poles and phase margin," in Proceedings of the 29th Chinese Control Conference, 2010.

[38] Taylor, M. D., "A compact series elastic actuator for bipedal robots with human-like dynamic performance," Master's thesis, Robotics Inst., Carnegie Mellon Univ., Pittsburgh, PA, USA, 2011.

[39] Thurfjell, L., McLaughlin, J., Mattsson, J., and Lammertse, P., "Haptic interaction with virtual objects: the technology and some applications", Industrial Robot: An International Journal, vol. 29, no. 3, pp. 210–215, 2002.

[40] Torres-Jara, E., and Banks, J., "A simple and scalable force actuator," presented at the Int. Symp. Robot., Paris, France, Mar. 2004.

[41] Wang, Z., "Interactive virtual prototyping of a mechanical system considering the environment effect. Part 1: Modeling dynamics", Comptes Rendus Mécanique, vol. 339, no. 9, pp. 591–604, 2011.

[42] Williamson, M., "Series elastic actuators" Master's thesis, Massachusetts Institute of Technology, 2000.